Journal of Alloys and Compounds 662 (2016) 612–620

Contents lists available at ScienceDirect

Journal of Alloys and Compounds

journal homepage: http://www.elsevier.com/locate/jalcom

Mössbauer spectroscopy, magnetic, and *ab-initio* study of the approximant $Al_{76}Ni_9Fe_{15}$ to a decagonal Al–Ni–Fe quasicrystal

Farshad Nejadsattari [a], Zbigniew M. Stadnik [a, *], Janusz Przewoźnik [b], Benjamin Grushko [c]

[a] Department of Physics, University of Ottawa, Ottawa, Ontario K1N 6N5, Canada
[b] Solid State Physics Department, Faculty of Physics and Applied Computer Science, AGH University of Science and Technology, 30-059 Kraków, Poland
[c] PGI-5 Forschungszentrum Jülich, D-52425 Jülich, Germany

ARTICLE INFO

Article history:
Received 24 November 2015
Accepted 14 December 2015
Available online 17 December 2015

Keywords:
Paramagnet
^{57}Fe Mössbauer spectroscopy
Electric quadrupole splitting
Pseudogap in the density of states
Debye temperature

ABSTRACT

The structural, magnetic, and Mössbauer spectral properties of the approximant $Al_{76}Ni_9Fe_{15}$ to a decagonal Al–Ni–Fe quasicrystal, complemented by *ab-initio* electronic structure and the hyperfine-interaction parameters calculations, are reported. The approximant studied crystallizes in the monoclinic space group $C2/m$ with the lattice parameters $a = 15.3898(3)$ Å, $b = 8.0840(2)$ Å, $c = 12.4169(2)$ Å, and $\beta = 107.870(2)^\circ$. The existence of a pseudogap in the calculated electronic density of states slightly above the Fermi level suggests electronic stabilization according to the Hume-Rothery-type mechanism. High metallicity of $Al_{76}Ni_9Fe_{15}$ is predicted. Both the Mössbauer spectra and magnetic susceptibility data indicate that $Al_{76}Ni_9Fe_{15}$ is a paramagnet down to 2.0 K. The presence of the distribution of the electric quadrupole splitting in the Mössbauer spectra measured in the temperature range 4.5–296.1 K is observed. The increase of the average quadrupole splitting with decreasing temperature is well described by a $T^{3/2}$ power-law relation. The Debye temperature of $Al_{76}Ni_9Fe_{15}$ is found to be 431(3) K.

1. Introduction

The most numerous class of quasicrystals (QCs) is that of icosahedral QCs [1]. The second, less numerous class of axial QCs [2] includes the decagonal QCs. The latter can be considered as being quasiperiodic in two dimensions and periodic in the third one, whereas the former have no periodicity along any direction.

The first observation of a metastable decagonal quasicrystalline phase $Al_{75}Ni_{10}Fe_{15}$ obtained by rapid solidification in the Al–Ni–Fe alloy system was reported by Tsai, Inoue and Masumoto [3]. This particular metastable decagonal phase was subsequently studied, mainly from structural point of view, in several publications [4–6]. It was shown [6–12] that other metastable decagonal QCs in the compositional range $Al_{70–75}Ni_{3–20}Fe_{10–22}$ could also be rapidly solidified. It was Lemmerz et al. [13] who discovered thermodynamically stable decagonal QCs in a narrow compositional range around $Al_{71}Ni_{24}Fe_5$. Structural and some physical properties of these high-quality decagonal Al–Ni–Fe QCs were studied in $Al_{71.5}Ni_{23.1}Fe_{5.4}$ [14], $Al_{71}Ni_{24}Fe_5$ [10,15–18], $Al_{71.6}Ni_{23.7}Fe_{4.7}$ [19], single-grain $Al_{70.1}Ni_{23.1}Fe_{5.7}$ [20,21], $Al_{71.5}Ni_{23.5}Fe_5$ [22–24], $Al_{71.6}Ni_{23.7}Fe_{4.7}$ [25], $Al_{73}Ni_{22}Fe_5$ [26], single-grain $Al_{72}Ni_{18}Fe_{10}$ [27,28], and $Al_{71.3}Ni_{24}Fe_{4.7}$ [29–32]. Very recently, the first natural decagonal QC with composition $Al_{71}Ni_{24}Fe_5$ has been discovered [33].

Studies of crystalline compounds, called approximants, play an important role in elucidating the local atomic structure of QCs and their corresponding physical properties. An approximant to a QC is a structurally complex crystalline compound, usually close in composition to the QC, that contains the arrangements of atoms in its large unit cell that closely approximate the local atomic structures in the QC [34–36]. $Al_{13}Fe_4$ has been identified [37] as an approximant to the metastable decagonal Al–Fe QC. As the crystal structure of $Al_{76}Ni_9Fe_{15}$ studied here is the same as that of $Al_{13}Fe_4$ [14], this comppound can be regarded as an approximant to a decagonal Al–Ni–Fe QC. Here we report the results of X-ray diffraction, ^{57}Fe Mössbauer spectroscopy, and magnetic study of $Al_{76}Ni_9Fe_{15}$, complemented by first-principles electronic structure and the hyperfine-interaction parameters calculations.

2. Experimental and theoretical methods

An ingot of nominal composition $Al_{76}Ni_9Fe_{15}$ was prepared by inductive melting constituent elements in a water-cooled copper

* Corresponding author.
E-mail address: stadnik@uottawa.ca (Z.M. Stadnik).

http://dx.doi.org/10.1016/j.jallcom.2015.12.115
0925-8388/

crucible under an argon atmosphere [14]. It was then annealed at 1073 K for 550 h and then water quenched.

X-ray diffraction measurements were carried out at 298 K in Bragg-Brentano geometry on a PANalytical X'Pert scanning diffractometer using Cu $K\alpha$ radiation in the 2θ range 2–120° in steps of 0.02°. The $K\beta$ line was eliminated by using a Kevex PSi2 Peltier-cooled solid-state Si detector.

The dc magnetization was measured in the temperature range from 2.0 to 350 K and in magnetic fields up to 90 kOe using the vibrating sample magnetometer (VSM) option of the Quantum Design physical property measurement system (PPMS). The dc magnetic susceptibility was measured using PPMS in the magnetic field of 10 kOe in the temperature range of 2–390 K.

The ^{57}Fe Mössbauer measurements [38] were conducted using a standard Mössbauer spectrometer operating in the sine mode and a ^{57}Co(Rh) source at room temperature. The spectrometer was calibrated with a 6.35-μm-thick α-Fe foil [39] and the spectra were folded. The Mössbauer absorber consisted of a mixture of powdered $Al_{76}Ni_9Fe_{15}$, and powdered boron nitride, which was pressed into a pellet and put into a high-purity, 8-μm-thick Al disk container to ensure a uniform temperature over the whole absorber. The Mössbauer absorber was put into a Mössbauer cryostat in which it was kept in a static exchange gas atmosphere at a pressure of ~ 6×10^{-3} mbar.

Ab initio electronic structure and Mössbauer hyperfine-interaction parameter calculations have been performed within the framework of density functional theory using the full-potential linearized augmented-plane-wave plus local orbitals (FP-LAPW+lo) method as implemented in the WIEN2k package [40]. In this method, one partitions the unit cell into two regions: a region of non-overlapping muffin-tin (MT) spheres centered at the atomic sites and an interstitial region. The wave functions in the MT regions are a linear combination of atomic radial functions times spherical harmonics, whereas in the interstitial regions they are expanded in plane waves. The basis set inside each MT sphere is split into a core and a valence subset. The core states are treated within the spherical part of the potential only and are assumed to have a spherically symmetric charge density in the MT spheres. The valence wave functions in the interstitial region were expanded in spherical harmonics up to $l = 4$, whereas in the MT region they were expanded to a maximum of $l = 12$ harmonics. For the exchange-correlation potential, the generalized gradient approximation (GGA) scheme of Perdew, Burke, and Ernzerhof [41] was used. A separation energy of −8.5 Ry between the valence and core states of individual atoms in the unit cell was chosen.

The values of 2.07, 1.20, and 1.03 a.u. were used as the MT radii for Fe, Ni, and Al, respectively. The plane-wave cut-off parameter was set to $R_{MT} \times K_{MAX} = 6.5$, where R_{MT} is the smallest MT radius in the unit cell and K_{MAX} is the maximum K vector used in the plane-wave expansion in the interstitial region. A total number of 432 k-points was used within a $9 \times 8 \times 12$ k-mesh in the irreducible wedge of the first Brillouin zone. A convergence criterion for self-consistent field calculations was chosen in such a way that the difference in energy between two successive iterations did not exceed 10^{-4} Ry. The experimental lattice parameters (a, b, c, and β) and the atomic position parameters (*vide infra*) were used in the calculations.

3. Results and discussion

3.1. Structural characterization

The studied compound $Al_{76}Ni_9Fe_{15}$, similarly to the $Al_{13}Fe_4$ compound, crystallizes in the monoclinic space group $C2/m$ (No. 12) [42]. Fig. 1 shows the crystal structure of $Al_{76}Ni_9Fe_{15}$. The rods connecting the Al, Ni, and Fe atoms (Fig. 1) describe the bonding between them (*vide infra*).

The x-ray powder diffraction pattern of $Al_{76}Ni_9Fe_{15}$ is shown in Fig. 2. A Rietveld refinement [43] of the x-ray powder diffraction data was carried out, yielding the lattice parameters $a = 15.3898(3)$ Å, $b = 8.0840(2)$ Å, $c = 12.4169(3)$ Å, and $\beta = 107.870(2)°$, and the atomic positional parameters that are listed in Table 1. The values of these lattice and atomic positional parameters are rather close to the corresponding values for $Al_{13}Fe_4$ [42,44]. We note that the Bragg peak at $2\theta \approx 39.3°$ (Fig. 2) must originate from a small amount of an unidentified second phase present in the sample studied.

3.2. Ab-initio calculations

3.2.1. Electronic structure

Fig. 3 shows the total and atom-resolved density of states (DOS) of $Al_{76}Ni_9Fe_{15}$. The non-zero DOS across a wide range from −10 to 10 eV with respect to the Fermi energy (E_F) is observed. No energy gaps within or outside of the Fermi region exist. A significant overlap between contributions to the DOS from Al and Fe over a wide energy range points to a metallic bonding between these atoms. This long-range and non-directional bonding is shown schematically in Fig. 1 with rods connecting the atoms in a unit cell. One can observe (Fig. 1) that every atom is connected to other atoms (either of the same or different type) in its environment in all directions and that this pattern is spread across the entire unit cell. Each of the 78 Al atoms within the unit cell contributes three electrons from the 3s and 3p orbitals to the system, giving rise to the metallic bonding and allowing the wave functions of these electrons to spread over large distances as compared to the atomic separations. The presence of a relatively large number of conduction electrons in $Al_{76}Ni_9Fe_{15}$ can explain good electrical and thermal conductivity of this compound. Other mechanisms, such as scattering of the free electrons by lattice vibrations at high temperatures, also contribute to the conductivity.

The total DOS is highly peaked (Fig. 3) in the energy region from −3.5 to −0.5 eV. It is dominated by the localized Fe d states, with a much smaller contribution from the Ni d states. As the most intense Ni states are peaked at lower energy than the corresponding Fe states, both of these states can be clearly observed in the total DOS. As mentioned earlier, a relatively high DOS above E_F originates mainly from the Al conduction electrons.

The remarkable feature of the calculated DOS (Fig. 3) is the existence of a deep minimum, or a pseudogap, centered at ~0.16 eV above E_F. This pseudogap is induced solely by the Fe states. The existence of such a pseudogap close to E_F is commonly interpreted as an electronic stabilization in term of the Hume-Rothery mechanism [45]. Whereas the existence of a pseudogap in the vicinity of E_F is an intrinsic feature of icosahedral QCs and their approximants [46–53], its presence was observed only in Al–Ni–Co and Al–Fe decagonal QCs and their approximants [54–58]. The presence of the pseudogap in the $Al_{76}Ni_9Fe_{15}$ approximant studied here suggests that it should also exist in the Al–Ni–Fe decagonal QCs.

The calculated band structure of $Al_{76}Ni_9Fe_{15}$ is shown in Fig. 4. The existence of numerous, highly packed energy bands accounts for a large number of accessible states, especially in the Fermi region. The high metallicity of $Al_{76}Ni_9Fe_{15}$ can be inferred from the fact that no energy band gap is seen across the Fermi level.

3.2.2. Charge density distribution

Fig. 5 shows the valence charge density distribution along two planes parallel to the ab plane. The presence of the charge density in the interatomic regions suggests a relatively good charge transport in the compound studied. The primitive unit cell of $Al_{76}Ni_9Fe_{15}$

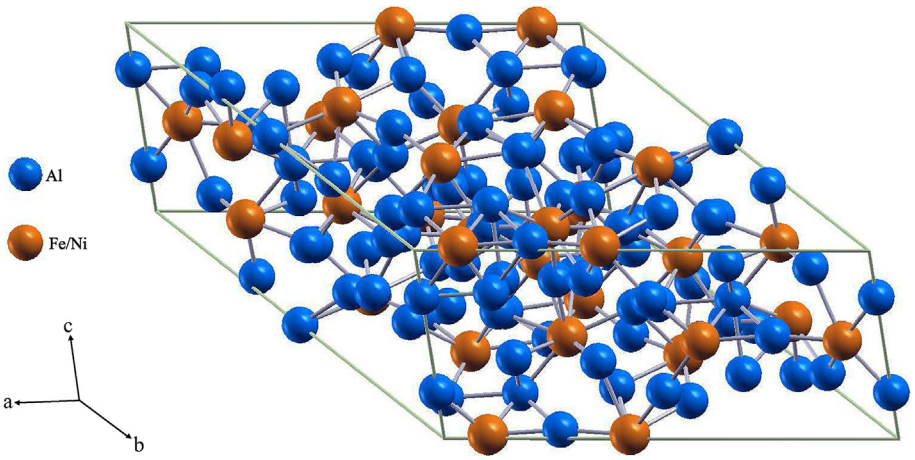

Fig. 1. The unit cell of the $Al_{76}Ni_9Fe_{15}$ compound.

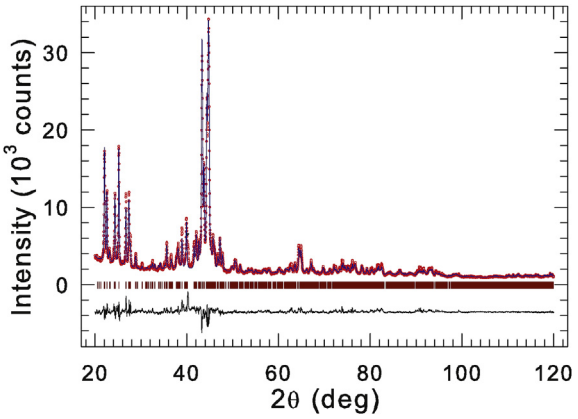

Fig. 2. Powder x-ray diffraction pattern of $Al_{76}Ni_9Fe_{15}$ at 298 K. The experimental data are denoted by open circles, while the line through the circles represents the results of the Rietveld refinement. The row of vertical bars shows the Bragg peak positions for the $C2/m$ space group. The lower solid line represents the difference curve between experimental and calculated patterns. The symbol ▽ indicates the Bragg peak position of an unidentified impurity phase.

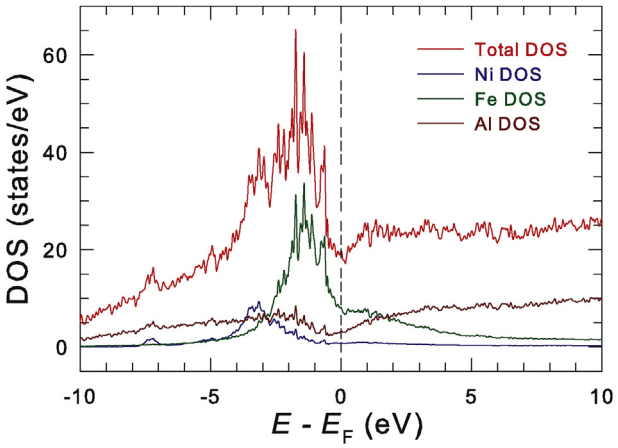

Fig. 3. Total and atom-resolved density of states of $Al_{76}Ni_9Fe_{15}$.

contains 102 atoms confined in the volume of 1470.3 Å^3. One can

Table 1
Atomic positions for the monoclinic $Al_{76}Ni_9Fe_{15}$ (space group $C2/m$) obtained through Rietveld analysis and calculated V_{zz} (in units of 10^{21} V/m^2) and η.

Atom	Site	Point symmetry	x	y	z	V_{zz}	η
0.625Fe(1)+0.375Ni(1)	4*i*	*m*	0.0825	0.0	0.3843	1.639	0.465
0.625Fe(2)+0.375Ni(2)	4*i*	*m*	0.3917	0.0	0.6306	3.803	0.531
0.625Fe(3)+0.375Ni(3)	4*i*	*m*	0.0897	0.0	0.9829	−0.148	0.781
0.625Fe(4)+0.375Ni(4)	4*i*	*m*	0.4019	0.0	0.9820	−0.065	0.366
0.625Fe(5)+0.375Ni(5)	8*j*	1	0.3172	0.2910	0.2762	−1.289	0.636
Al(1)	4*i*	*m*	0.0622	0.0	0.1795	1.714	0.789
Al(2)	4*i*	*m*	0.3270	0.0	0.2870	−0.752	0.192
Al(3)	4*i*	*m*	0.2419	0.0	0.5381	−3.724	0.408
Al(4)	4*i*	*m*	0.0721	0.0	0.5628	1.356	0.741
Al(5)	4*i*	*m*	0.2410	0.0	0.9600	−5.266	0.280
Al(6)	4*i*	*m*	0.4797	0.0	0.8320	−1.205	0.819
Al(7)	2*d*	2/*m*	$\frac{1}{2}$	0.0	$\frac{1}{2}$	−0.794	0.273
Al(8)	4*i*	*m*	0.2971	0.0	0.7727	−0.389	0.394
Al(9)	4*i*	*m*	0.0935	0.0	0.7982	−3.009	0.337
Al(10)	8*j*	1	0.1828	0.2205	0.1088	−0.421	0.423
Al(11)	8*j*	1	0.3697	0.2081	0.1141	−1.536	0.272
Al(12)	8*j*	1	0.8135	0.7899	0.6605	−3.411	0.553
Al(13)	8*j*	1	0.4862	0.2245	0.3324	3.736	0.733
Al(14)	8*j*	1	0.3683	0.2009	0.4781	−1.123	0.576
Al(15)	4*g*	2	0.0	0.2474	0.0	4.382	0.796

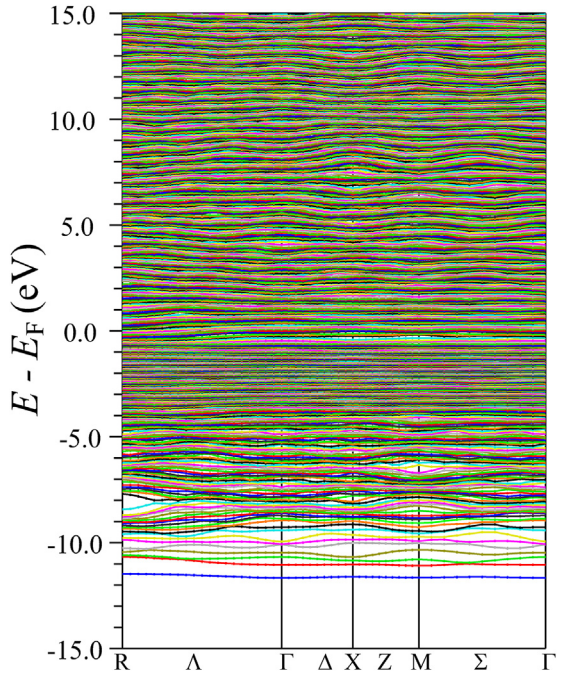

Fig. 4. Energy band structure of $Al_{76}Ni_9Fe_{15}$.

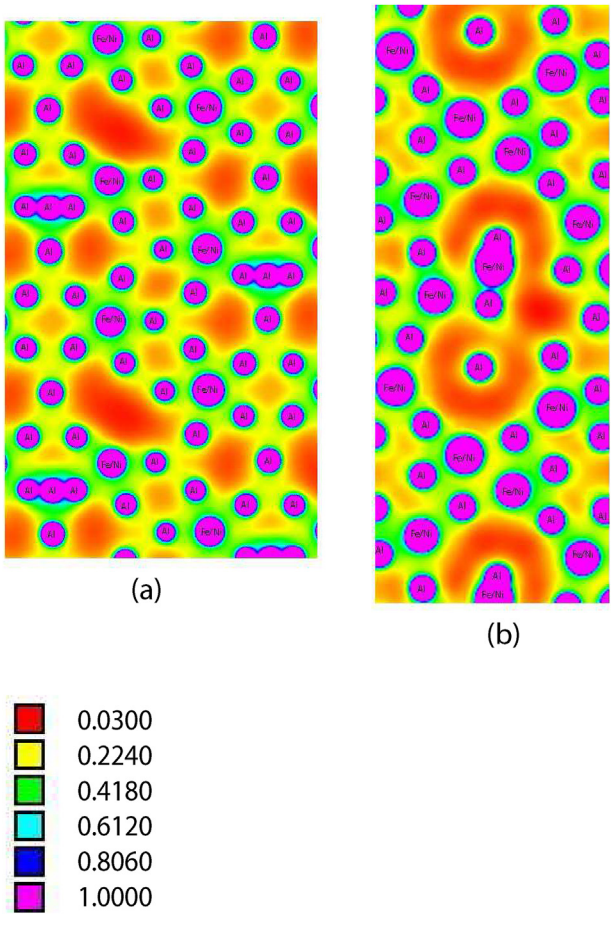

Fig. 5. Electron charge density distribution (in units of e/Å^3) along the $z = 0.726$ plane (a) and the $z = 0.5$ plane (b).

see from Fig. 1 that on average the atoms are evenly distributed in the unit cell, with a slight preference of occupying the volume between the $z = 0.247$ and $z = 0.753$ planes. Thus, on average every atom occupies a volume of 14.4 Å^3, that is, the average separation between the atoms is about 2.43 Å. This relatively small distance between the atoms in $Al_{76}Ni_9Fe_{15}$ leads to a strong Coulomb interaction between them, which results in the formation of regions with high charge density. The hybridization between the Fe/Ni and Al states can also be observed in Fig. 5 as high charge-density regions, which supports the earlier comments made based on the calculated DOS.

3.2.3. Hyperfine interaction parameters

Numerical analysis of Mössbauer spectra of a paramagnetic compound yields the two most important hyperfine-interaction parameters: the quadrupole splitting (the separation between two resonance lines in a ^{57}Fe Mössbauer quadrupole doublet) $\Delta = \frac{1}{2}eQ|V_{zz}|\sqrt{1+\eta^2/3}$, where e is the proton charge, Q is the electric quadrupole moment of the ^{57}Fe nucleus (0.15 b) [59], V_{zz} is the principal component of the electric field gradient (EFG) tensor, and η is the asymmetry parameter, and the isomer shift, δ_0 [38]. If the crystal structure of a compound studied is known, V_{zz}, η, and δ_0 can be also obtained from first-principles calculations [60]. The calculated V_{zz} and η values are displayed in Table 1 and their comparison with experiment will be discussed below.

The isomer shift $\delta_0 = \alpha[\rho(0) - \rho_{ref}(0)]$ results from the difference in the total electron density at the Mössbauer nucleus in the compound studied, $\rho(0)$, and in the reference compound, $\rho_{ref}(0)$; α is a calibration constant. In calculating $\rho(0)$, relativistic spin-orbit effects were invoked in order to account for the possibility of the penetration of the $p_{1/2}$ electrons into the ^{57}Fe nuclei. An α-Fe (with the *bcc* structure and the lattice constant of 2.8665 Å) was chosen as a reference compound. The calculated value of $\rho_{ref}(0)$ is 15309.918 a.u.$^{-3}$. The calculated values of $\rho(0)$ at the first five crystallographic sites (Table 1) are 15308.901, 15309.231, 15309.092, 15308.996, and 15309.068 a.u.$^{-3}$.

3.3. Mössbauer spectroscopy

We measured first the room- and liquid-nitrogen temperature ^{57}Fe Mössbauer spectra of $Al_{76}Ni_9Fe_{15}$ over a large velocity range (Fig. 6) in order to identify a possible pattern originating from an Fe-containing magnetic impurity phase. In addition to a quadrupole doublet of the main phase that results from a distribution of quadrupole splittings (*vide infra*), no Zeeman pattern originating from a possible magnetic impurity phase present in the studied specimen can be discerned in the spectra (Fig. 6). In other words, if the compound studied does contain Fe-based magnetic impurity phase, its amount must be below the ^{57}Fe Mössbauer spectroscopy detection limit.

In order to evaluate how reliable the calculations of Δ and δ_0 for $Al_{76}Ni_9Fe_{15}$ are, a theoretical 0.0 K Mössbauer spectrum was generated. The calculated values of V_{zz} and η at the first five crystallographic sites (Table 1) lead to the following values of Δ: 0.265, 0.621, 0.025, 0.010, and 0.225 mm/s. Using the calibration constant $\alpha = -0.291$ a.u.^{3}(mm/s) [61], the calculated values of $\rho(0)$ (*vide supra*) lead to the following δ_0 values: 0.296, 0.200, 0.240, 0.268, and 0.247 mm/s. With these δ_0 and Δ values, a Mössbauer spectrum was generated and compared with the spectrum at 4.5 K [Fig. 7(a)]. One observes a significant disagreement between these two spectra. In particular, the isomer shift of the theoretical spectrum is much lower than that of the experimental spectrum. If one allows only for the δ_0 values to be fitted, a reasonable agreement between the two spectra is achieved [Fig. 7(b)]. The disagreement between the calculated and measured Δ and δ_0 parameters is probably

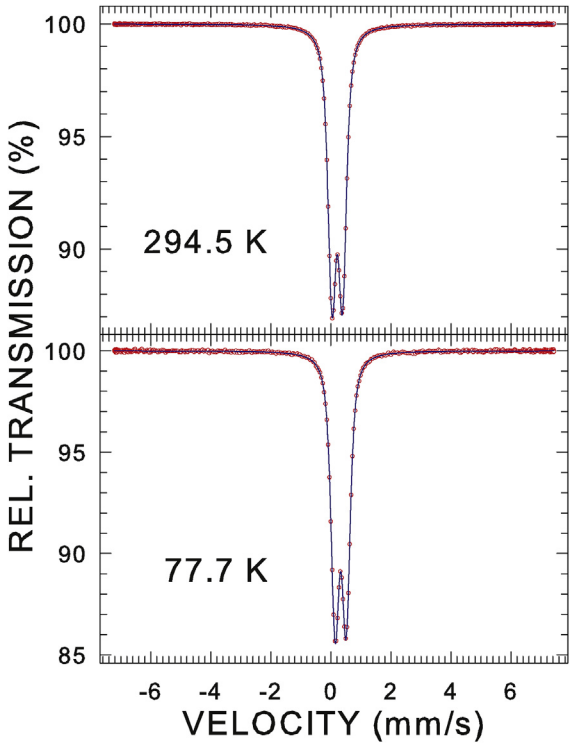

Fig. 6. Room- and liquid-nitrogen temperature ^{57}Fe Mössbauer spectra of $Al_{76}Ni_9Fe_{15}$ measured in a large velocity range fitted (blue solid line) with a distribution of quadrupole splittings, as described in the text. The zero-velocity origin is relative to α-Fe at room temperature (For interpretation of the references to color in this figure legend, the reader is referred to the web version of this article.).

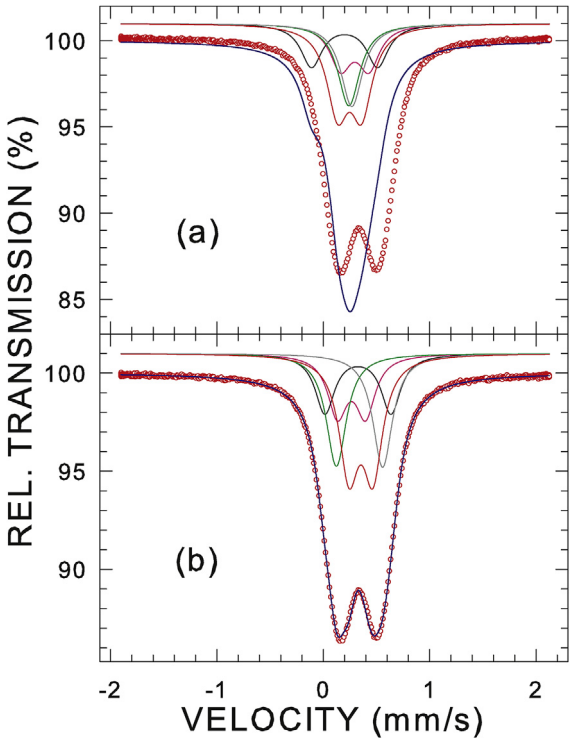

Fig. 7. (Color online) (a) ^{57}Fe Mössbauer spectrum of $Al_{76}Ni_9Fe_{15}$ at 4.5 K and simulated spectrum (blue solid line) resulting from the superposition of five quadrupole doublets (with the calculated δ_0 and Δ values) due to the Fe atoms at the Fe(1) site (pink solid line), Fe(2) site (black solid line), Fe(3) site (green solid line), Fe(4) site (dark gray solid line), and Fe(5) site (red solid line) (b) The same as in (a) but with fitted δ_0 values (For interpretation of the references to color in this figure legend, the reader is referred to the web version of this article.).

related to the fact that the calculations were carried out for an ordered compound. However, the Fe and Ni atoms in the compound studied are distributed randomly at the first five crystallographic sites. This should lead to the distributions of δ_0 and Δ, rather than to the single δ_0 and Δ values at these sites.

The Mössbauer spectra of $Al_{76}Ni_9Fe_{15}$ recorded at temperatures between 4.5 and 296.1 K are shown in Fig. 8. They do not exhibit the expected three-valley structure characteristic of the spectra of the structurally similar Al_{13} Fe_4 compound [62]. All the spectra are in the form of a broadened quadrupole doublet which results from the presence of a distribution $P(\Delta)$ of the quadrupole splitting Δ [63]. The Mössbauer spectra in Fig. 8 were fitted with the Voight-based quadrupole distribution method of Rancourt and Ping [64]. To account for a small asymmetry of the spectra, a linear coupling between the center shift, δ, and Δ for the elementary Lorentzian doublets was assumed [64,65]. The best fits of the Mössbauer spectra in Fig. 8 could be obtained with the distributions $P(\Delta)$ shown in Fig. 9.

The average value of the quadrupole splitting, $\overline{\Delta}$, at a given temperature was calculated from the $P(\Delta)$ distribution at that temperature (Fig. 9) and is shown in Fig. 10. One can note a clear increase of $\overline{\Delta}$ with decreasing temperature. The temperature dependence of $\overline{\Delta}$ could be fitted well (Fig. 10) to the empirical equation

$$\overline{\Delta}(T) = \overline{\Delta}(0)\left(1 - BT^{3/2}\right), \tag{1}$$

where $\overline{\Delta}(0)$ is the value of $\overline{\Delta}$ at 0 K and B is a constant. Such a $T^{3/2}$ temperature dependence has been observed in many crystalline [62,66], quasicrystalline [67], and amorphous [68] compounds. This seemingly universal $T^{3/2}$ dependence is not well understood. Its origin seems to be associated with a strong temperature dependence of mean-square lattice displacements and, to a lesser extent, with the temperature dependence of the lattice parameters [69]. The of values of $\overline{\Delta}(0)$ and B determined from the fit of the $\overline{\Delta}(T)$ data (Fig. 10) to Eq. (1) are, respectively, 0.379(3) mm/s and $1.24(3) \times 10^{-5}$ $K^{-3/2}$. The value of B found here is similar to the values found for other compounds [62,66–68].

The absence of the magnetic dipole hyperfine interaction [38] in the Mössbauer spectra of $Al_{76}Ni_9Fe_{15}$ (Fig. 8) proves that the compound studied has no long-range magnetic order down to 4.5 K, i.e., that it is a paramagnet. The paramagnetic nature of $Al_{76}Ni_9Fe_{15}$ will be confirmed by the magnetic measurements (*vide infra*).

The temperature dependence of the average value of the center shift $\overline{\delta}$ (relative to α-Fe at 298 K), determined from the fits of the Mössbauer spectra in Fig. 8, is shown in Fig. 11(a). The $\overline{\delta}(T)$ dependence is given by

$$\overline{\delta}(T) = \delta_0 + \delta_{SOD}(T), \tag{2}$$

where δ_0 is the intrinsic isomer shift and $\delta_{SOD}(T)$ is the second-order Doppler (SOD) shift which depends on lattice vibrations of the Fe atoms [38]. In terms of the Debye approximation of the lattice vibrations, $\delta_{SOD}(T)$ is expressed in terms of the Debye temperature, Θ_D, as

$$\delta_{SOD}(T) = -\frac{9}{2}\frac{k_B T}{Mc}\left(\frac{T}{\Theta_D}\right)^3 \int_0^{\Theta_D/T} \frac{x^3 dx}{e^x - 1}, \tag{3}$$

where k_B is the Boltzmann constant, M is the mass of the Mössbauer

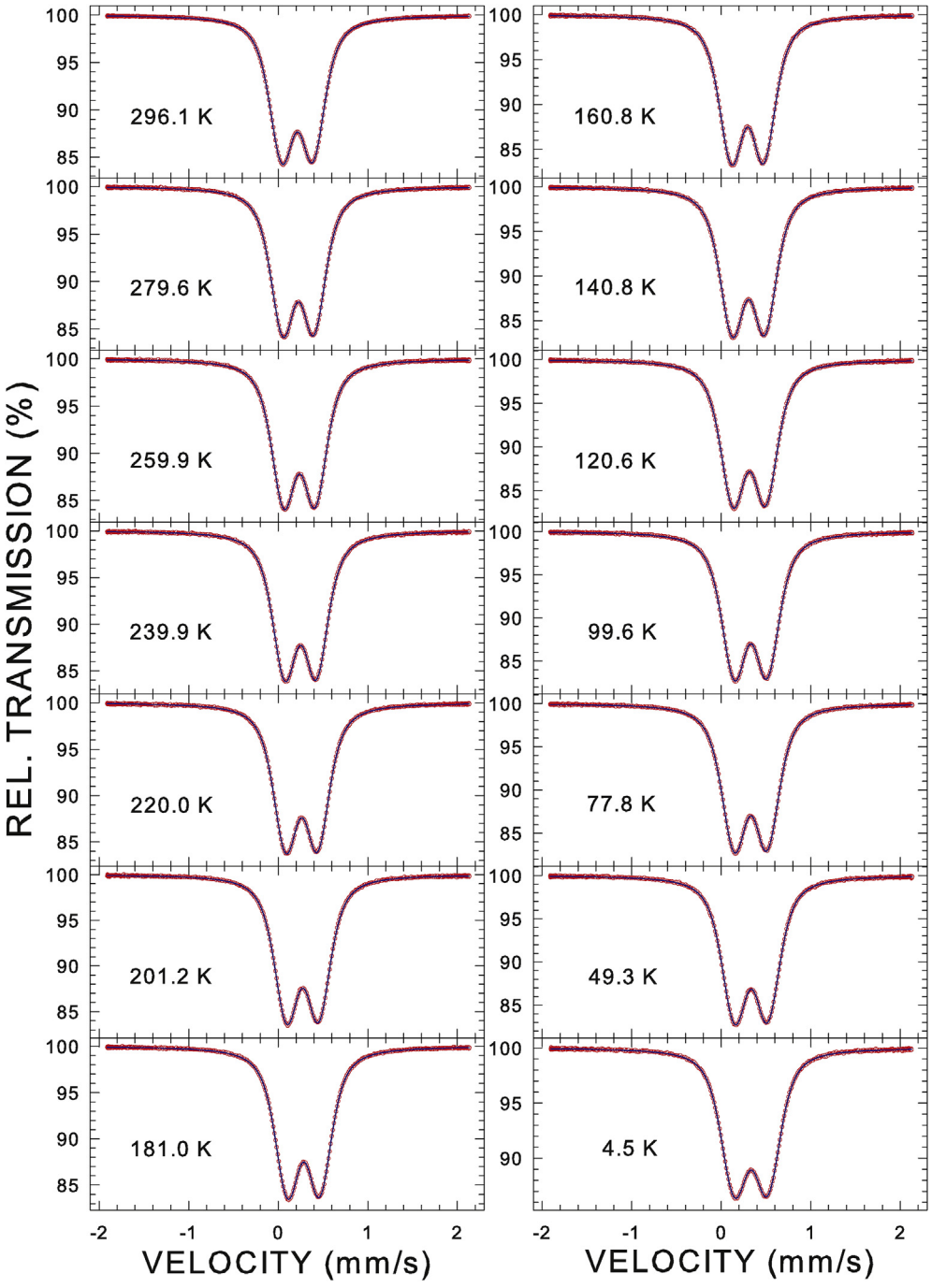

Fig. 8. ^{57}Fe Mössbauer spectrum of $Al_{76}Ni_9Fe_{15}$ at the indicated temperatures fitted (blue solid lines) with the quadrupole splitting distributions $P(\Delta)$ shown in Fig. 9. The zero-velocity origin is relative to α-Fe at room temperature (For interpretation of the references to color in this figure legend, the reader is referred to the web version of this article.).

nucleus, and c is the speed of light. By fitting the experimental data $\overline{\delta}(T)$ [Fig. 11(a)] to Eq. (2), the quantities δ_0 and Θ_D were found to be, respectively, 0.333(1) mm/s and 430(5) K.

There is another method of determining the Debye temperature from Mössbauer spectroscopy data. Fig. 11(b) displays the temperature dependence of the absorption spectral area, A, derived from the fits of the Mössbauer spectra in Fig. 8. This area is proportional to the absorber Debye-Waller factor f_a, which is given in the Debye theory [38] by

$$f_a(T) = \exp\left\{ -\frac{3}{4}\frac{E_\gamma^2}{Mc^2 k_B \Theta_D}\left[1 + 4\left(\frac{T}{\Theta_D}\right)^2 \int_0^{\Theta_D/T} \frac{x\,dx}{e^x - 1}\right]\right\}, \quad (4)$$

where E_γ is the energy of the Mössbauer transition. The fit of the $A(T)$ data [Fig. 11(b)] to Eq. (4) yields $\Theta_D = 432(3)$ K. This value of Θ_D is very close to the value of 430(5) K derived from the $\overline{\delta}(T)$ dependence. The weighted average of the above two Θ_D values determined from the temperature dependence of two different physical parameters is 431(3) K. This Θ_D value is slightly higher

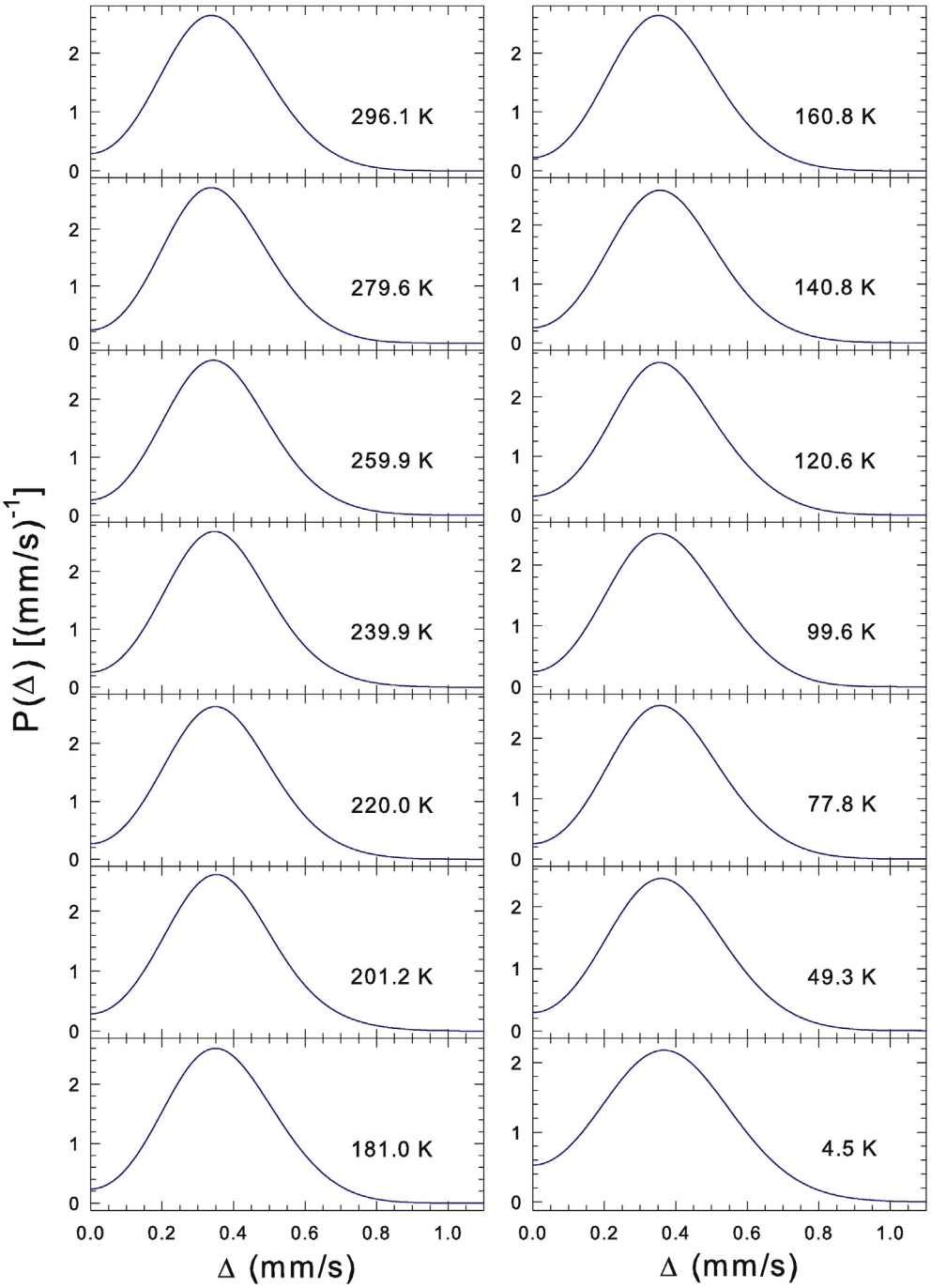

Fig. 9. (Color online) The quadrupole splitting distributions $P(\Delta)$ which fit best the ^{57} Fe Mössbauer spectra in Fig. 8.

than the value of 383(3) K of the structurally similar $Al_{13}Fe_4$ compound [62].

3.4. Magnetic measurements

In spite of the fact that the Mössbauer spectra in Figs. 6 and 8 show no presence of a possible magnetic impurity in the specimen studied (at the level of ~ 1 wt%), the magnetic field dependence of magnetization curves $M(H)$ measured at selected temperatures (Fig. 12) are typical for a ferromagnet. The $M(H)$ curves do not saturate in the highest field available of 90 kOe. It must be concluded that the specimen studied does contain a ferromagnetic impurity (at the ppm concentration level), probably in the form of an iron-oxide phase at the sample's surfaces or precipitated iron superparamagnetic clusters.

The temperature dependence of the magnetic susceptibility χ of $Al_{76}Ni_9Fe_{15}$ measured in an applied magnetic field of 10 kOe is shown in Fig. 13(a). It follows approximately (because of the presence of a tiny amount of ferromagnetic impurity) a $1/T$-like dependence. The $\chi(T)$ data above 250 K [Fig. 13(a)] were fitted to a modified Curie-Weiss law

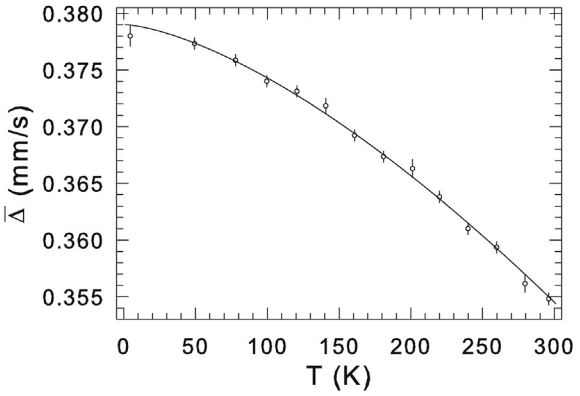

Fig. 10. Temperature dependence of the average quadrupole splitting of $Al_{76}Ni_9Fe_{15}$. The solid line is the fit to Eq. (1), as explained in the text.

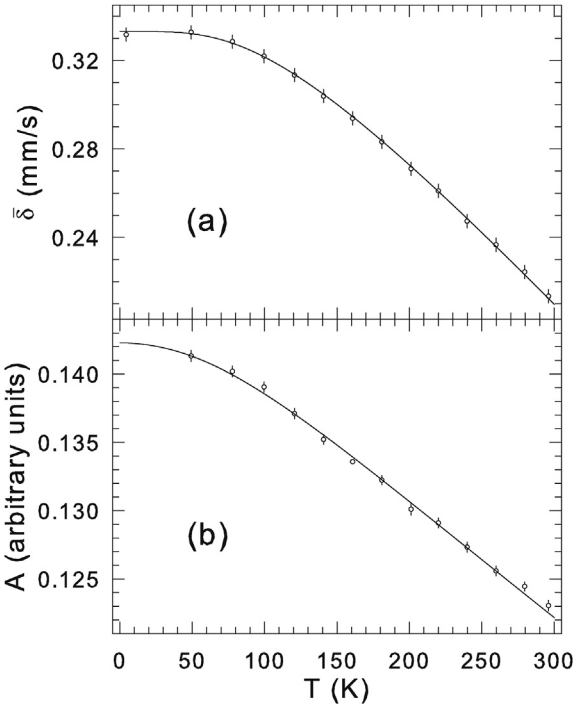

Fig. 11. Temperature dependence of (a) the average center shifts $\bar{\delta}$ and (b) the absorption spectral area *A*. The solid lines are the fits to Eq. (2) in (a) and to Eq. (4) in (b), as explained in the text.

$$\chi = \chi_0 + \frac{C}{T - \Theta_p}, \tag{5}$$

where χ_0 is the temperature-independent term that includes contributions from Pauli and Van Vleck paramagnetism as well as core and Landau diamagnetism, *C* is the Curie constant, and Θ_p is the paramagnetic Curie temperature. The Curie constant can be expressed as $C = \frac{N\mu_{eff}^2}{3k_B}$, where *N* is the number of transition metal (TM) atoms per formula unit, and μ_{eff} is the effective magnetic moment. The fit of the $\chi(T)$ data to Eq. (5) gives $\chi_0 = -5.85(31) \times 10^{-6}$ cm^3/g, $C = 5.15(25) \times 10^{-3}$ cm^3 K/g, and $\Theta_p = -99(10)$ K. Fig. 13(b) shows the inverse magnetic susceptibility corrected for the contribution χ_0 as $(\chi - \chi_0)^{-1}$ versus temperature; the validity of the modified Curie-Weiss law is conformed. The value of *C* corresponds to $\mu_{eff} = 2.42(6)\ \mu_B$ per TM atom. The unusually small value of Θ_p indicates the antiferromagnetic interaction between the TM atoms.

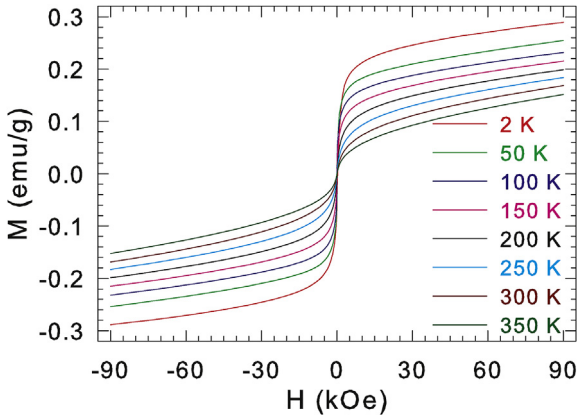

Fig. 12. Hysteresis curves of $Al_{76}Ni_9Fe_{15}$ at selected temperatures in the magnetic field range −90 – +90 kOe.

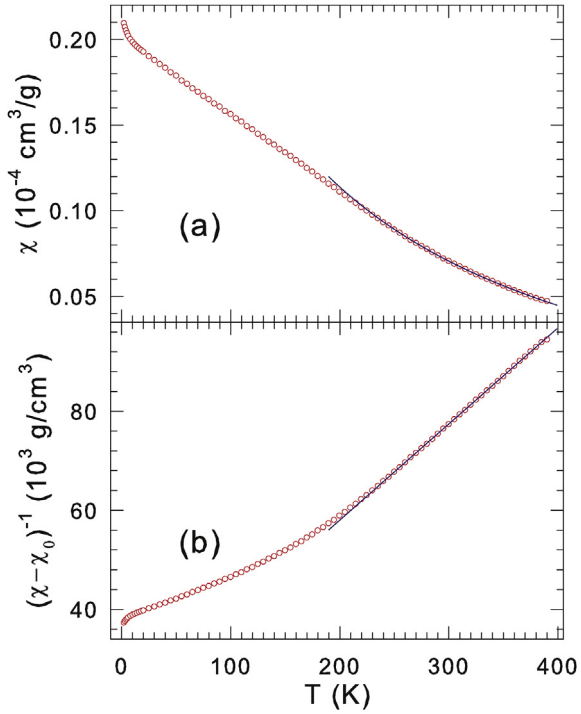

Fig. 13. (a) Temperature dependence of the magnetic susceptibility of $Al_{76}Ni_9Fe_{15}$ measured in an external magnetic field of 10 kOe. The solid line is the fit to Eq. (5) in the temperature range 250–390K, as explained in the text. (b) Temperature dependence of the inverse magnetic susceptibility corrected for the contribution χ_0, $(\chi - \chi_0)^{-1}$. The solid line is the fit to Eq. (5).

4. Summary

The results of x-ray diffraction, ^{57} Fe Mössbauer spectroscopy, and magnetic measurements, complemented by *ab-initio* electronic structure and the hyperfine-interaction parameters calculations, of the approximant $Al_{76}Ni_9Fe_{15}$ to a decagonal Al–Ni–Fe quasicrystal are presented. The compound studied is shown to crystallize in the monoclinic space group *C*2/*m* with the lattice parameters $a = 15.3898(3)$ Å, $b = 8.0840(2)$ Å, $c = 12.4169(2)$ Å, and $\beta = 107.870(2)^\circ$. The calculated DOS reveals the existence of a

pseudogap slightly above the Fermi energy, which points to a possible contribution of the Hume-Rothery mechanism to the stabilization of the structure. Good metallicity of $Al_{76}Ni_9Fe_{15}$ is predicted. The Mössbauer spectra measured in the temperature range 4.5–296.1 K reveal the presence of a distribution of the electric quadrupole splitting. The decrease of the average quadrupole splitting with temperature is well accounted for by a $T^{3/2}$ power–law relation. The compound studied is shown to be a paramagnet down to 2.0 K. The Debye temperature of $Al_{76}Ni_9Fe_{15}$ is found to be 431(3) K.

Acknowledgments

This work was supported by the Natural Sciences and Engineering Research Council of Canada.

References

[1] Z.M. Stadnik (Ed.), Physical Properties of Quasicrystals, Springer-Verlag, Berlin, 1999. Quasicrystals, An Introductions to Structure, Physical Properties, and Applications, edited by J.-B. Suck, M. Schreiber, and P. Häussler (Springer-Verlag, Berlin, 2002); Quasicrystals, edited by T. Fujiwara and Y. Ishii (Elsevier, Amsterdam, 2008).
[2] W. Steurer, Z. Krist. 219 (2004) 391.
[3] A.-P. Tsai, A. Inoue, T. Masumoto, Mater. Trans. Jpn. Inst. Met. 30 (1989) 150.
[4] A.P. Tsai, N. Kataoka, A. Inoue, T. Masumoto, Jpn. J. Appl. Phys. 29 (1990) L1696.
[5] Z. Zhang, Y. Zhuang, Philos. Mag. Lett. 65 (1992) 203.
[6] R.A. Dunlap, Philos. Mag. B 67 (1993) 69.
[7] M. Saito, M. Tanaka, A.P. Tsai, A. Inoue, T. Masumoto, Jpn. J. Appl. Phys. 31 (1992) L109.
[8] K. Tsuda, M. Saito, M. Terauchi, M. Tanaka, A.P. Tsai, A. Inoue, T. Masumoto, Jpn. J. Appl. Phys. 32 (1993) 129.
[9] M. Tanaka, K. Tsuda, M. Terauchi, A. Fujiwara, A.P. Tsai, A. Inoue, T. Masumoto, J. Non-Cryst. Solids 153–154 (1993) 98.
[10] Z.M. Stadnik, B. Grushko, A.P. Tsai, in: S. Takeuchi, T. Fujiwara (Eds.), Proceedings of the 6th International Conference on Quasicrystals, World Scientific, Singapore, 1998, p. 708.
[11] M. Saito, K. Tsuda, M. Tanaka, A.P. Tsai, Jpn. J. Appl. Phys. 38 (1999) L671.
[12] T. Yokosawa, K. Saitoh, M. Tanaka, A.P. Tsai, J. Alloys Compd. 342 (2002) 169.
[13] U. Lemmerz, B. Grushko, C. Freiburg, M. Jansen, Philos. Mag. Lett. 69 (1994) 141.
[14] R. Würschum, T. Troev, B. Grushko, Phys. Rev. B 52 (1995) 6411.
[15] B. Grushko, U. Lemmerz, K. Fisher, C. Freiburg, Phys. Stat. Sol. A 155 (1996) 17.
[16] D. Holland-Moritz, I.-R. Lu, G. Wilde, J. Schroers, B. Grushko, J. Non-Cryst. Solids 250–252 (1999) 829.
[17] M. Döblinger, R. Witmann, B. Grushko, J. Alloys Compd. 360 (2003) 162.
[18] A. Yasuhara, K. Yamamoto, K. Yubuta, K. Hiraga, Acta Phys. Pol. A 126 (2014) 637.
[19] K. Hiraga, K. Yubuta, K.T. Park, J. Mater. Res. 11 (1996) 1702.
[20] T. Drobek, R.W. Stark, M. Gräber, W.M. Heckl, New J. Phys. 1 (1999) 15.1.
[21] T. Drobek, W.M. Heckl, Mater. Sci. Eng. 294–296 (2000) 878.
[22] F. Frey, Mater. Sci. Eng. 294–296 (2000) 178.
[23] E. Weidner, J.-L. Lei, F. Frey, R. Wang, B. Grushko, J. Alloys Compd. 342 (2002) 156.
[24] E. Weidner, F. Frey, J.L. Lei, B. Pedersen, C. Paulmann, W. Morgenroth, J. Appl. Cryst. 37 (2004) 802.
[25] K. Hiraga, T. Ohsuna, Mater. Trans. JIM 42 (2001) 894.
[26] K. Saitoh, M. Tanaka, A.P. Tsai, J. Electron Microsc. 50 (2001) 197.
[27] H. Abe, K. Yamamoto, S. Matsuoka, Y. Matsuo, J. Phys. Condens. Matter 19 (2007) 466201.
[28] H. Abe, H. Saitoh, H. Nakao, K. Yamamoto, Philos. Mag. 91 (2011) 2491.
[29] P.P. Parshin, M.G. Zemlyanov, R.A. Brand, Crystallogr. Rep. 52 (2007) 436.
[30] P.P. Parshin, M.G. Zemlyanov, G. Kh Panova, A.A. Shikov, R.A. Brand, B. Grushko, JETP 109 (2009) 645.
[31] G.Kh Panova, M.G. Zemlyanov, P.P. Parshin, A.A. Shikov, R.A. Brand, Phys. Solid State 52 (2010) 771.
[32] P.P. Parshin, M.G. Zemlyanov, R.A. Brand, Crystallogr. Rep. 56 (2011) 1145.
[33] L. Bindi, N. Yao, C. Lin, L.S. Hollister, C.L. Andronicos, V.V. Distler, M.P. Eddy, A. Kostin, V. Kryachko, G.J. MacPherson, W.M. Steinhardt, M. Yudovskaya, P.J. Steinhardt, Sci. Rep. 5 (2015) 9111.
[34] V. Elser, C.L. Henley, Phys. Rev. Lett. 55 (1985) 2883.
[35] A.I. Goldman, K.F. Kelton, Rev. Mod. Phys. 65 (1993) 213.
[36] Z.M. Stadnik, in: K.H.J. Buschow (Ed.), Handbook of Magnetic Materials, vol. 21, Elsevier, Amsterdam, 2013, p. 77.
[37] T. Fujiwara, T. Yokokawa, Phys. Rev. Lett. 66 (1991) 333.
[38] N.N. Greenwood, T.C. Gibb, Mössbauer Spectroscopy, Chapman and Hall, London, 1971. P. Gütlich, E. Bill, and A. Trautwein, Mössbauer Spectroscopy and Transition Metal Chemistry (Springer, Berlin, 2011).
[39] J.P. Cali (Ed.), Certificate of Calibration, Iron Foil Mössbauer Standard, Natl. Bur. Stand. (U.S.) Circ. No. 1541, 1971. U.S. GPO, Washington, D.C.,.
[40] P. Blaha, K. Schwartz, G. Madsen, D. Kvasnicka, J. Luitz, WIEN2k, an Augmented Plane Wave Plus Local Orbitals Program for Calculating Crystal Properties, Karlheinz Schwarz, Technical Universität Wien, Austria, 1999.
[41] J.P. Perdew, S. Burke, M. Ernzerhof, Phys. Rev. Lett. 77 (1996) 3865.
[42] J. Grin, U. Burkhardt, M. Ellner, K. Oeters, Z. Krist. 209 (1994) 479.
[43] R.A. Young, The Rietveld Method, Oxford University Press, Oxford, 1993.
[44] P. Popčević, A. Smontara, J. Ivkov, M. Wencka, M. Komelj, P. Jeglič, S. Vrtnik, M. Bobnar, Z. Jagličić, B. Bauer, P. Gille, H. Borrmann, U. Burkhardt, Yu Grin, J. Dolinšek, Phys. Rev. B 81 (2010) 184203.
[45] G. Trambly de Laissardière, D. Nguyen-Manh, D. Mayou, Prog. Mater. Sci. 50 (2005) 679.
[46] Z.M. Stadnik, D. Purdie, M. Garnier, Y. Bauer, A.-P. Tsai, A. Inoue, K. Edagawa, S. Takeuchi, Phys. Rev. Lett. 77 (1996) 1777.
[47] Z.M. Stadnik, D. Purdie, M. Garnier, Y. Bauer, A.-P. Tsai, A. Inoue, K. Edagawa, S. Takeuchi, K.H.J. Buschow, Phys. Rev. B 55 (1997) 10938.
[48] Z.M. Stadnik, D. Purdie, T.A. Lograsso, Phys. Rev. B 64 (2001) 214202.
[49] R. Tamura, Y. Murao, S. Takeuchi, T. Kiss, T. Yokoya, S. Shin, Phys. Rev. B 65 (2002) 224202.
[50] A. Suchodolskis, W. Assmus, L. Giovanelli, U.O. Karlsson, V. Karpus, G. Le Lay, E. Sterzel, E. Uhrig, Phys. Rev. B 68 (054207) (2003).
[51] R. Widmer, P. Gröning, M. Feuerbacher, O. Gröning, Phys. Rev. B 79 (2009) 104202.
[52] H.R. Sharma, G. Simutis, V.R. Dhanak, P.J. Nugent, C. Cui, M. Shimoda, R. McGrath, A.P. Tsai, Y. Ishii, Phys. Rev. B 81 (2010) 104205.
[53] J. Nayak, M. Maniraj, A. Gloskovskii, M. Krajčí, S. Sebastian, I.R. Fisher, K. Horn, S.R. Barman, Phys. Rev. B 91 (2015) 235116.
[54] T. Suzuki, H.R. Sharma, T. Nishimura, M. Shimoda, Y. Yamauchi, A.P. Tsai, Phys. Rev. B 72 (2005) 115427.
[55] M. Krajčí, J. Hafner, M. Kihalkovič, Phys. Rev. B 73 (2006) 134203.
[56] K.H. Hassdenteufel, A.R. Oganov, S. Katrych, W. Steurer, Phys. Rev. B 75 (2007) 144115.
[57] T. Mertelj, A. Ošlak, J. Dolinšek, I.R. Fisher, V.V. Kabanov, D. Mihailovic, Phys. Rev. Lett. 102 (2009) 086405.
[58] M.A. Albedah, F. Nejadsattari, Z.M. Stadnik, J. Przewoźnik, J. Alloys Compd. 619 (2015) 839.
[59] G. Martínez-Pinedo, P. Schwerdtfeger, E. Caurier, K. Langanke, W. Nazarewich, T. Söhnel, Phys. Rev. Lett. 87 (2001) 062701.
[60] P. Blaha, J. Phys. Conf. Ser. 217 (012009) (2010).
[61] U.D. Wdowik, K. Reubenbauer, Phys. Rev. B 76 (2007) 155118.
[62] M.A. Albedah, F. Nejadsattari, Z.M. Stadnik, J. Przewoźnik, J. Alloys Compd. 619 (2014) 839.
[63] Z.M. Stadnik, in: G.J. Long, F. Grandjean (Eds.), Mössbauer Spectroscopy Applied to Magnetism and Materials Science, vol. 2, Plenum, New York, 1996, p. 125.
[64] D.G. Rancourt, J.Y. Ping, Nucl. Instrum. Methods Phys. Res. B 58 (1991) 85.
[65] S.J. Campbell, F. Aubertin, in: G.J. Long, F. Grandjean (Eds.), Mössbauer Spectroscopy Applied to Inorganic Chemistry, vol. 3, Plenum, New York, 1989, p. 183.
[66] E.N. Kaufmann, R.H. Vianden, Rev. Mod. Phys. 51 (1979) 161 and references therein; P. Wang, Z. M. Stadnik, J. Żukrowski, A. Thaler, S. L. Bud'ko, and P. C. Canfield, Phys. Rev. B 84, 024509(2011); Z. M. Stadnik, P. Wang, J. Żukrowski, T. Noji, and Y. Koike, J. Phys.: Condens. Matter 25, 416008 (2013); M. A. Albedah, K. Al-Qadi, Z. M. Stadnik, and J. Przewoźnik, J. Alloys Compd. 613, 344 (2014).
[67] K. Al-Qadi, P. Wang, Z.M. Stadnik, J. Przewoźnik, Phys. Rev. B 79 (2009) 224202. Z. M. Stadnik and G. Zhang, J. Phys.: Condens. Matter 17, 6599(2005); Z. M. Stadnik, T. Takeuchi, N. Tanaka, and U. Mizutani, J. Phys.: Condens. Matter 15, 6365 (2003).
[68] Z.M. Stadnik, Ö Rapp, V. Srinivas, J. Saida, A. Inoue, J. Phys. Condens. Matter 14 (2002) 6883. M. Mao, D. H. Ryan, and Z. Altounian, Hyperfine Interact. 92, 2163(1994); P. Deppe and M. Rosenberg, Hyperfine Interact. 15-16, 735 (1993).
[69] K. Nishiyama, F. Dimmling, Th Kornrumph, D. Riegel, Phys. Rev. Lett. 37 (1976) 357. J. Christiansen, P. Heubes, R. Keitel, W. Klinger, W. Loeffler, W. Sandner, W. Witthuhn, Z. Phys. B 24, 177(1976); P. Jena, Phys. Rev. Lett. 36, 418 (1976); K. W. Lodge, J. Phys. F 9, 2035 (1979).